Differential Expression of Syndecan-1 Mediates Cationic Nanoparticle Toxicity in Undifferentiated versus Differentiated Normal Human Bronchial Epithelial Cells

Haiyuan Zhang,[△,†] Tian Xia,[△,‡] Huan Meng,[‡] Min Xue,[§] Saji George,[†,‡] Zhaoxia Ji,[†] Xiang Wang,[†] Rong Liu,[⊥] Meiying Wang,[‡] Bryan France,[#] Robert Rallo,[⊥] Robert Damoiseaux,[†,∥] Yoram Cohen,[⊥] Kenneth A. Bradley,[†,∥] Jeffrey I. Zink,[§] and Andre E. Nel[†,‡,*]

[†]California NanoSystems Institute, [‡]Division of NanoMedicine, Department of Medicine, [§]Department of Chemistry & Biochemistry, [⊥]Department of Chemical & Biomolecular Engineering, [∥]Molecular Shared Screening Resources, and [#]Department of Microbiology, Immunology & Molecular Genetics, University of California, Los Angeles, California, United States. [△] Contributed equally to this work.

ABSTRACT Most *in vitro* toxicity studies on engineered nanomaterials (ENMs) use transformed rather than primary cells for logistical reasons. However, primary cells may provide a more appropriate connection to *in vivo* toxicity because these cells maintain their phenotypic fidelity and are also capable of differentiating into lineages that may be differently affected by potentially hazardous ENMs. Few studies to date have focused on the role of cellular differentiation in determining ENM toxicity. We compared the response of undifferentiated and differentiated primary human bronchial epithelial (NHBE) cells to cationic mesoporous silica nanoparticles (MSNPs) that are coated with polyethyleneimine (PEI) since this polymer is known to exert differential cytotoxicity depending on its molecular weight and cationic density. The attachment of cationic PEI polymers to the MSNP surface was used to assess these materials' toxicological potential in undifferentiated and differentiated human bronchial epithelial cells, using a multiparametric assay that screens for an integrated set of sublethal and lethal response outcomes. MSNPs coated with high molecular weight (10 and 25 kD) polymers were more toxic in differentiated cells than particles coated with shorter length polymers. The increased susceptibility of the differentiated cells is in agreement with more abundant expression of a proteoglycan, syndecan-1, which contains copious heparin sulfate side chains. Pretreatment with heparinase to remove the negatively charged sulfates decreased MSNP—PEI binding to the cell surface and lowered the cytotoxic potential of the cationic particles. These data demonstrate the importance of studying cellular differentiation as an important variable in the response of primary cells to toxic ENM properties.

KEYWORDS: cationic nanoparticles · polyethyleneimine (PEI) · toxicity · differentiation · primary epithelial cells

Recent advances and progress in nanobiotechnology have demonstrated the potential of engineered nanomaterials (ENMs) as drug or gene carriers,[1,2] biosensors,[3,4] and biomedical imaging reagents.[5,6] Widespread use of ENMs in consumer products has introduced the possibility that these materials come into contact with humans and the environment and could lead to adverse health or biological effects.[7] A full understanding of the biological hazard of ENMs requires addressing the material properties that could lead to hazard generation.[8] This information is also required for the safer design of ENMs through modification properties such as material redox potential, particle dissolution with shedding of toxic ions, or engaging in membrane or lysosomal damage due to cationic surface charge.[7,9]

In this article we were interested in further exploring the role of cationic surface charge in primary human bronchial epithelial cells because of the previous documentation that inhalation of cationic spray paint particles can lead to bronchiolitis obliterans and acute pulmonary edema in humans.[10] The use of normal human bronchial epithelial (NHBE) cells allows the assessment of cationic nanoparticle toxicity in both their differentiated and undifferentiated states, an aspect of primary cellular behavior that has not been systematically explored in nanotoxicology studies and is of considerable importance in considering nanomaterial impact on tissues capable of undergoing differentiation such as epithelia, the neuronal system, bone marrow lineages, and the immune system. As an example, the rate of cellular apoptosis in response to cadmium telluride quantum dots is much higher in differentiated than undifferentiated murine neuroblastoma cells.[11] In order to facilitate a study on the differentiation status of NHBE cells, we have developed a mesoporous silica nanoparticle

* Address correspondence to anel@mednet.ucla.edu.

Received for review November 23, 2010 and accepted February 23, 2011.

Published online March 02, 2011
10.1021/nn200328m

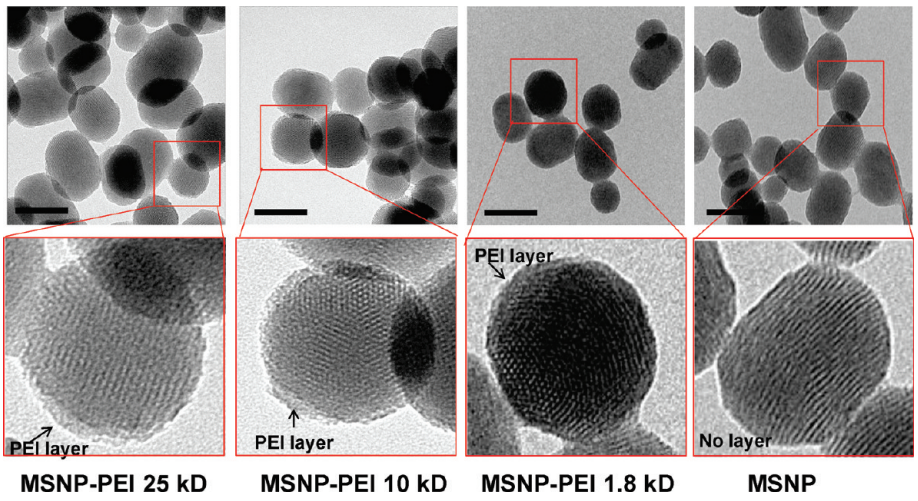

Figure 1. TEM images of PEI−MSNPs. TEM images were obtained prior to and after coating with the 25, 10, and 1.8 kD PEI polymer. The bottom panels show that the pores on the coated and uncoated particles remain open. Other PEI-coated particles had the same appearance. Scale bar, 100 nm.

(MSNP) library in which surface coating with cationic polyethyleneimine (PEI) results in exaggerated toxicity in cancer or transformed cells exposed to particles coated with longer length polymers and displaying increased cationic density.[12] Moreover, we have implemented a multiparametric cellular screening assay that allows an integrated and rapid throughput assessment of sublethal and lethal cellular response outcomes that are displayed through heat map analysis (Figure S1).[13−16] This high-throughput assay assesses contemporaneously oxygen radical generation, intracellular Ca^{2+} flux, mitochondrial depolarization, and increased membrane permeability (Figure S1). Our analysis demonstrated that MSNPs coated with longer length PEI polymers are more toxic in NHBE cells than particles coated with shorter length polymers. We also observed that differentiated NHBE cells exhibit increased cellular association and toxicity compared to undifferentiated cells. The increased cytotoxicity in differentiated cells is concordant with a higher surface expression of the anionic heparan sulfate proteoglycan syndecan-1. In order to determine whether these events are linked, we used heparinase treatment to strip heparan sulfates from the surface of differentiated and undifferentiated NHBE cells and could show that this leads to a significant decrease in cationic nanoparticle cytotoxicity in differentiated but not undifferentiated cells. These data suggest that heparan sulfate expression is an important cellular target for the binding of cationic nanoparticles, thereby rendering differentiated bronchial epithelial cells more susceptible to the toxicological impact of cationic functionalization.

RESULTS

Physicochemical Characterization of Polyethyleneimine (PEI)-Coated MSNPs. MSNPs were coated with branched PEI polymers that varied from 0.6 to 25 kD in size (Figure 1).[12] The base particle size is 100−130 nm and is prepared with a phosphonate-coated surface. This anionic group is used for electrostatic binding of the PEI polymers, which constitutes 11.5−16.1% of the total particle mass by thermogravimetric analysis (Table S1). While the average suspended particle size was ∼200−300 nm in water and increased to ∼2200 nm in basic epithelial growth medium (BEGM), the addition of 2 mg/mL BSA was capable of stabilizing the average particle size at ∼1000 nm in the same growth medium (Table 1). We have previously shown that this level of BSA supplementation improves MSNP stability during epithelial experimentation.[13,14] This dispersal can be further improved by including 10% fetal calf serum (FCS) in the BEGM medium, as demonstrated by shrinking of the average particle size to 250−310 nm (Table 1). While the PEI-coated MSNPs exhibited a positive zeta potential in water, the addition of BSA or FCS was accompanied by a negative zeta potential as a result of being coated by negatively charged proteins (Table 2). However, in spite of attracting a negatively charged protein corona, the inner particle surface maintains protonated amines that are capable of interacting with anionic groups that are capable of competing with BSA.[17]

Differentiation of Normal Human Bronchial Epithelial (NHBE) Cells. Primary NHBE cells are cultured in retinoic acid (RA) to prevent cellular differentiation.[18−21] Removal of the RA supplement from NHBE cells leads to their differentiation into a spindle-shaped instead of a ellipsoid phenotype (Figure 2A).[22] To further define the state of differentiation through biomarker expression, we also looked at the expression of small proline-rich (SPR) and β-catenin proteins, which showed increased expression in differentiated compared to undifferentiated cells (Figure 2B).[23,24] We refer to the ellipsoid, SPR-2 negative, low β-catenin expressing as

TABLE 1. MSNP Average Sizes As Determined by DLS

	size (nm)			
MSNP−PEI and MSNPs	H_2O	BEGM 10% serum	BEGM (2 mg/mL BSA) (with RA)	BEGM (2 mg/mL BSA) (without RA)
MSNP−PEI 25 kD	224.5 ± 3	319.3 ± 19	1218.7 ± 320	937.0 ± 212
MSNP−PEI 10 kD	195.4 ± 14	284.7 ± 17	1548.0 ± 363	1240.5 ± 399
MSNP−PEI 1.8 kD	209.7 ± 40	250.5 ± 38	1248.0 ± 143	905.4 ± 137
MSNP−PEI 1.2 kD	229.8 ± 39	306.0 ± 31	1092.6 ± 238	1118.1 ± 279
MSNP−PEI 0.8 kD	275.2 ± 17	324.5 ± 49	1172.0 ± 69	972.9 ± 150
MSNP−PEI 0.6 kD	222.5 ± 13	285.6 ± 10	1172.0 ± 120	903.2 ± 141
MSNP	263.3 ± 2	258.2 ± 23	409.3 ± 33	370.1 ± 108

TABLE 2. MSNP Zeta Potential in Different Solutions[a]

	zeta potential (mV)			
MSNP−PEI and MSNPs	H_2O	BEGM 10% serum	BEGM (2 mg/mL BSA) (with RA)	BEGM (2 mg/mL BSA) (without RA)
MSNP−PEI 25 kD	+68.6 ± 0.7	−9.4 ± 1	−7.8 ± 3	−10.7 ± 3
MSNP−PEI 10 kD	+70.5 ± 0.5	−15.0 ± 1	−8.7 ± 1.5	−8.8 ± 1
MSNP−PEI 1.8 kD	+71.1 ± 2	−12.3 ± 2	−9.4 ± 3.3	−8.9 ± 2.3
MSNP−PEI 1.2 kD	+70.9 ± 2	−10.3 ± 2	−4.2 ± 1	−14.0 ± 4
MSNP−PEI 0.8 kD	+62.0 ± 1	−10.2 ± 4	−14.4 ± 2	−8.6 ± 2
MSNP−PEI 0.6 kD	+73.2 ± 0.6	−15.5 ± 1	−11.9 ± 4	−11.6 ± 2
MSNP	−56.3 ± 2	−11.2 ± 1	−10.3 ± 3	−11.8 ± 3

[a] Compared to the values in water, there is a statistically significant decrease in the zeta potential of cationic MSNP after the addition of 10% FCS ($p < 0.05$) or BSA ($p < 0.05$).

undifferentiated cells, while the spindle-shaped, SPR-2 positive, and β-catenin positive cells are regarded as differentiated cells.

Undifferentiated and Differentiated NHBE Cells Display Different Response Profiles to Cationic MSNP in the Multiparametric Assay. A multiparametric assay was performed in undifferentiated and differentiated cells exposed to PEI-coated as well as noncoated MSNPs over a wide dose range (0.4−200 μg/mL) and for time periods ranging from 1 to 6 h. This assay detects five different responses that are being tracked by fluorescent dyes, namely, intracellular calcium flux (Fluo-4), surface membrane leakage (PI uptake), increased H_2O_2 generation (DCF), increased superoxide generation (MitoSox Red), and decreased mitochondrial membrane potential (JC-1 fluorescence).[16] The automated assay assesses the change in cellular fluorescence intensity above a certain threshold, which scores the % positive cells for each parameter (a description of the threshold determination appears in the Materials and Methods section). Statistical analysis of the epifluorescence data was performed by a strictly standard mean difference (SSMD) method, which assesses the significantly different responses between the treated and nontreated cells.[25,26] These data were used to generate heat maps in which a red display signifies significant toxicity, while green denotes no significant response differences. The heat map shown in Figure 3 demonstrates that PEI-coated particles induce stronger PI and MitoSox Red responses than cells loaded with Fluo-4, DCF, and JC-1. Moreover, the high molecular weight PEI polymers (10 and 25 kD) elicited stronger responses than coating with shorter length polymers or the phosphonate control. A further finding of interest was that the particles coated with the longer length (10 and 25 kD) polymers elicited stronger responses in NHBE cells in their differentiated state (Figure 3). While undifferentiated cells showed minimal effects in the first 4 h, the response intensity increased by the fifth and sixth hour. Independent displays of the PI and MitoSox Red responses in Figure S2A and S2B demonstrate that while 30−40% of the differentiated cells are positive for PI uptake and 20−50% are positive for MitoSox Red, <5% of the undifferentiated cells respond to particles coated with the 10 and 25 kD polymers. Similar results were obtained in a transformed human bronchial epithelial cell line, BEAS-2B, as well as a transformed rat type I alveolar epithelial cell line, R3/1, in which the higher molecular weight polymers also produced more PI uptake (Figure S3A) and MitoSox Red fluorescence (Figure S3B). All considered, the multiparametric analysis shows that bronchial and alveolar epithelial cell toxicity is determined by PEI polymer length and that differentiated NHBE cells are more vulnerable to cationic MSNP than undifferentiated cells. This is a novel observation and of considerable importance to the use of materials with cationic properties for nanotherapy because cationic nanoparticles have frequently been associated with adverse health affects in animal studies.[27]

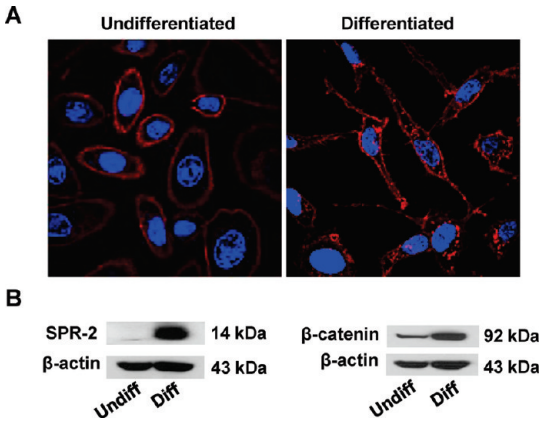

Figure 2. Confocal microscopy showing the undifferentiated and differentiated cell morphologies in parallel with immunoblotting results for epithelial differentiation markers. (A) Confocal microscopy showing difference in cellular morphology in undifferentiated (left) and differentiated cells (right). The cell membrane was stained by Alexa Fluor 594-conjugated wheat germ agglutinin (WGA) and nuclei stained by Hoechst 33342. Cells were visualized under a Leica confocal 1P/FCS microscope. (B) Immunoblotting analysis comparing SPR-2 and β-catenin expression in undifferentiated and differentiated cells relative to the household pattern, β-actin.

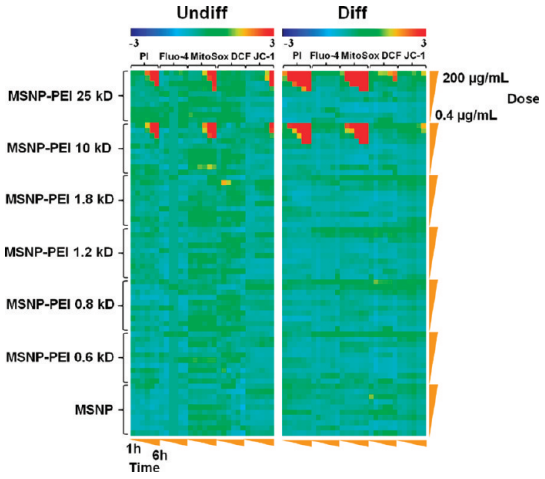

Figure 3. Heat map to compare the toxicity of various PEI-coated particles in undifferentiated and differentiated NHBE cells by a rapid throughput multiparametric assay. The heat map was established using SSMD statistical analysis to evaluate significant differences in the toxicological response profiles of undifferentiated and differentiated NHBE cells. The response parameters included in the multiparametric assay include measurement of intracellular calcium flux (Fluo-4), superoxide generation (MitoSox Red), H_2O_2 generation (DCF), and mitochondrial membrane depolarization (JC-1). Cells were treated by MSNP−PEI or MSNP at doses of 0.4, 0.8, 1.6, 3.2, 6.3, 12.5, 25, 50, 100, and 200 μg/mL. Epifluorescence images were collected hourly for 6 h. The layout of the 384-well plate used in this experimentation is shown in Figure S7. Full details of the multiparametric assay, preparation of the particles, and processing of the plate appear in Materials and Methods. The fluorescent dyes are displayed in Table 3.

Differential Cellular Association of Cationic MSNP with Undifferentiated and Differentiated Cells. Our own previous studies using NH_2-conjugated polystyrene (PS) nanoparticles

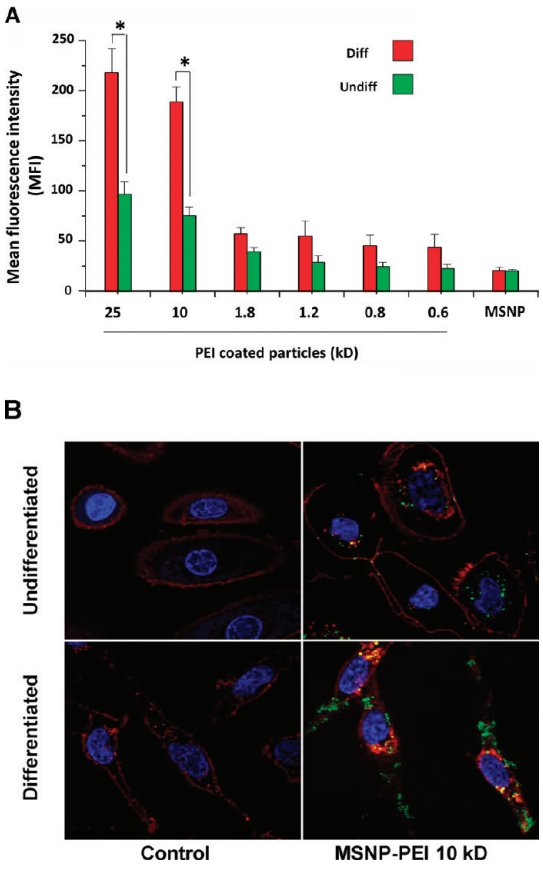

Figure 4. Differential cellular association of FITC-labeled MSNP−PEI in undifferentiated and differentiated NHBE cells. (A) FITC-labeled, PEI-coated MSNPs (25 μg/mL) were used to determine cellular association at 3 h by flow cytometry and confocal microscopy. The flow measurement used mean fluorescence intensity (MFI) units to study the cellular association of the particles. The MFI of the particles coated with the 10 and 25 kD polymers is significantly higher in differentiated cells compared to undifferentiated cells. (B) Confocal microscopy images showing the cellular localization of FITC−MSNP−PEI 10 kD in undifferentiated and differentiated cells. A significant fraction of the labeled particles are attached to the surface membrane of differentiated cells. *$p < 0.05$ compared with control.

demonstrated that in the size range < 90 nm their cellular toxicity could be attributed to a high rate of cellular association, cellular uptake, and lysosomal damage compared to neutral particles.[13,15] In order to study possible differences in the cellular association of FITC-labeled MSNP in undifferentiated and differentiated cells, we used flow cytometry and confocal microscopy for making these comparisons. Following the addition of FITC-labeled MSNP (25 μg/mL) for 3 h and calculating the units of mean fluorescence intensity (MFI), flow cytometry analysis showed that particle coating with the 10 and 25 kD polymers induced a significant increase in MSNP association with differentiated cells (Figure 4A).

Similar results were obtained when using particles that were better dispersed through supplementation of BEGM with 10% FCS (Figure S4A), demonstrating that the effects of cationic particles of ~300 nm size are

the same as those of larger agglomerates (FCS was excluded in further experiments because of its potential to induce epithelial cell differentiation). Cellular toxicity (% PI positive cells) also varied in accordance with the cellular association (Figures 4B and S4B). Whether dispersed by BSA or FCS, cellular association of shorter length (0.6−1.8 kD) PEI-coated particles was clearly less than particles coated with longer length (10 and 25 kD) polymers (Figures 4A and S4A). In order to demonstrate the role of cationic charge in the cellular association and toxicity, PEI amine groups were neutralized by phthalic anhydride. This neutralization was confirmed by the decrease of the positive zeta potential (Table S2). Decreased cationic charge and cellular association were accompanied by decreased toxicity (Figure S5). Please notice that although BSA binding to the cationic particle surface leads to a negative zeta potential in supplemented media, the BSA-coated particle surface maintains protonated amines that are capable of interacting with anionic charges on the cell surface, as demonstrated by the decrease in cell-associated fluorescence after neutralization of the amines in Figure S5. Thus, at the contact site of the particle surface with the cell membrane, the cationic groups likely compete for binding to anionic membrane components that could replace the protein corona. The density distribution of the protonated amines is important in shaping these short length membrane interactions, as demonstrated by colloidal flocculation studies carried out using different size PEI polymers.[28] This may explain the increased cytotoxic potential of the higher molecular weight polymers and the reduction in toxicity when these interactive amines are neutralized by phthalic anhydride (Figure S5).

In order to further confirm the flow cytometry data, confocal microscopy looked at the cellular association of FITC-labeled particles (Figure 4B). While only a few particles can be observed interiorly in undifferentiated cells, differentiated cells showed an abundance of particles, most of which appear to be attached to the surface membrane (Figure 4B). The likely reason for increased membrane association in differentiated cells is the presence of a high-affinity membrane component that interacts with the cationic particles, as will be explained below.

Cationic MSNPs Affect Surface Membrane Potential in Differentiated Cells and Can Hemolyze Red Blood Cells (RBC). Strong particle association with the surface membrane in differentiated cells could lead to surface membrane perturbation. In order to more directly probe cationic effects on membrane function, we assessed the influence on the membrane potential, using a fluorescence-based approach that involves a lipophilic, anionic bis-oxonol dye. This dye shows increased cellular fluorescence during membrane depolarization or a reduction in fluorescence intensity during membrane hyperpolarization. Differentiated cells had a significant reduction in membrane potential when exposed to the particles coated with 10 and 25 kD polymers (Figure 5A). Comparative effects in undifferentiated cells were minor (Figure 5A). Noncoated particles or particles coated with the 1.8 kD polymer had little or no effect on membrane potential (Figure 5A). In addition to disrupting membrane potential, cationic nanoparticles have also been shown to disrupt membrane integrity.[29] In order to test that possibility, we performed a red cell lysis assay that utilizes mouse RBC.[29] This demonstrated a dose-dependent increase in hemoglobin release by MSNP-PEI 10 kD but no effect by noncoated particles (Figure 5B). The same result was obtained with the 25 kD polymer. All considered, the data in Figures 4 and 5 suggest that the binding of particles coated with the higher molecular weight polymers induced membrane perturbation and cytotoxicity in differentiated cells.

Heparinase Treatment Decreases NP Cellular Association and MSNP−PEI Toxicity. Cellular differentiation is accompanied by altered expression of heparan sulfate proteoglycans (HSPGs) and glycosaminoglycans at the surface membrane of epithelial cells.[30,31] These negatively charged components play a role in cellular attachment of positively charged submicrometer silica particles.[32] Heparinase treatment of differentiated NHBE cells prior to introduction of FITC-labeled MSNP (25 μg/mL) showed a 6.4-fold or 6.8-fold decrease in cellular association of cationic particles coated with 10 or 25 kD polymers, respectively (Figure 6A). This was accompanied by a 3.4-fold or 3.7-fold decrease in PI uptake in heparinase-treated cells (Figure 6B). Confocal microscopy confirmed that fewer particles were bound to the differentiated cells after treatment with heparinase (Figure 6C). All considered, the data in Figure 6 suggest that HSPG expression plays a role in cationic particle toxicity in differentiated NHBE cells.

Increased Syndecan-1 Expression and Co-localization with Fluorescent Cationic MSNP in Differentiated NHBE Cells. It has been reported that HSPGs act as cell-surface receptors for PEI-mediated polyplexes.[33−35] This protein family includes a diverse range of molecules, including syndecans,[36] betaglycan,[37] CD44v3,[38] and glypicans.[39] Among these, the syndecans (syndecans 1−4) constitute the most abundant HSPGs and play a central role in cellular differentiation.[40] Since syndecan-1 is particularly relevant to epithelial cells,[32] we assessed its expression in undifferentiated and differentiated NHBE cells, using confocal microscopy and immunoblotting. Utilizing an anti-human syndecan-1 monoclonal antibody together with FITC-labeled goat anti-mouse IgG secondary antibody, we could show that syndecan-1 is actively expressed on the surface of differentiated cells, as confirmed by WGA co-staining (Figure 7A). Similar results were obtained by immunoblotting (Figure 7B). Moreover, in a follow-up experiment FITC-labeled MSNP coated with a 10 kD PEI polymer co-localized with syndecan-1, which was detected with an Alexa Fluor

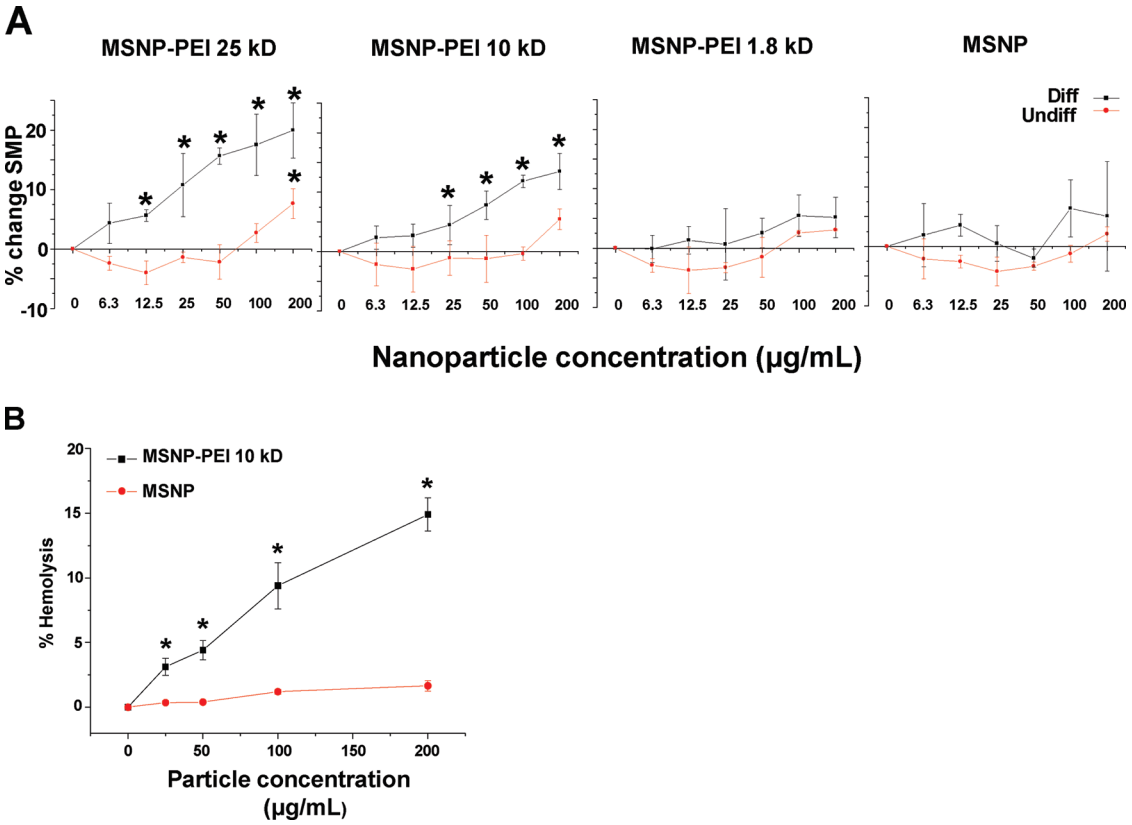

Figure 5. Surface membrane depolarization and the RBC hemolysis by cationic MSNP. (A) Assessment of surface membrane potential (SMP) using a fluorescence assay in which differentiated cells incubated with MSNP−PEI 25 kD and 10 kD and labeled with the FMP dye show a significant loss of membrane potential. The same particles had minimal effects in undifferentiated cells. Particles coated with the 1.8 kD polymer or noncoated particles had little effect. These data are in agreement with the cytotoxicity analysis in Figure 3. (B) Hemolysis assay using mouse RBCs: while MSNP−PEI 10kD showed dose-dependent hemolysis (up to 14.9% of RBC) over the concentration range 25−200 μg/mL, noncoated particles were without an effect. *$p < 0.05$ compared with control.

594-conjugated antibody (Figure 8). The degree of co-localization was 64.3%, as determined by Image J software analysis.

DISCUSSION

In the present study, we compared the toxicological response of cationic MSNP coated with different length PEI polymers in undifferentiated and differentiated NHBE cells. Particles coated with the 10 and 25 kD PEI polymers showed increased cellular association compared to lesser cationic particles. Moreover, differentiated cells showed more toxicity than undifferentiated cells in a multiparametric assay that assesses sublethal and lethal cellular responses. The increased susceptibility of differentiated cells was associated with increased expression of the proteoglycan, syndecan-1, on the cell surface. Syndecan-1 contains abundant anionic heparan sulfate groups that are capable of binding to the cationic MSNP. Pretreatment with heparinase lowered particle association as well as cytotoxicity in differentiated cells. In addition to triggering intracellular responses and cytotoxicity, cationic particles lowered the membrane potential of differentiated NHBE cells and affected the structural integrity of the RBC membrane, suggesting that the surface-bound particles trigger membrane responses that contribute to cationic particle toxicity. This constitutes the first report, to our knowledge, showing a selective difference in the response of undifferentiated and differentiated cells to a cationic nanomaterial and is of importance in assessing the safety of therapeutic nanomaterials, where the cationic charge has been identified as an important characteristic leading to ENM toxicity.[27]

The *in vitro* assessment of ENM safety is often carried out in transformed cell lines that are inexpensive to grow and homogeneous and yield reproducible results.[41] However, transformed cells are genetically altered and differ in important aspects from primary cell types, e.g., number of chromosomes, cellular household, growth potential, biological responsiveness, regulation of viability pathways, and the use of signal transduction pathways. Moreover, transformed cell lines are less informative in cellular screening studies used in drug discovery, while primary cells are more informative of biological outcomes at the *in vivo* level.[42] Primary cells are also capable of differentiating into separate lineages that could be differentially affected by potentially harmful materials. In the present study,

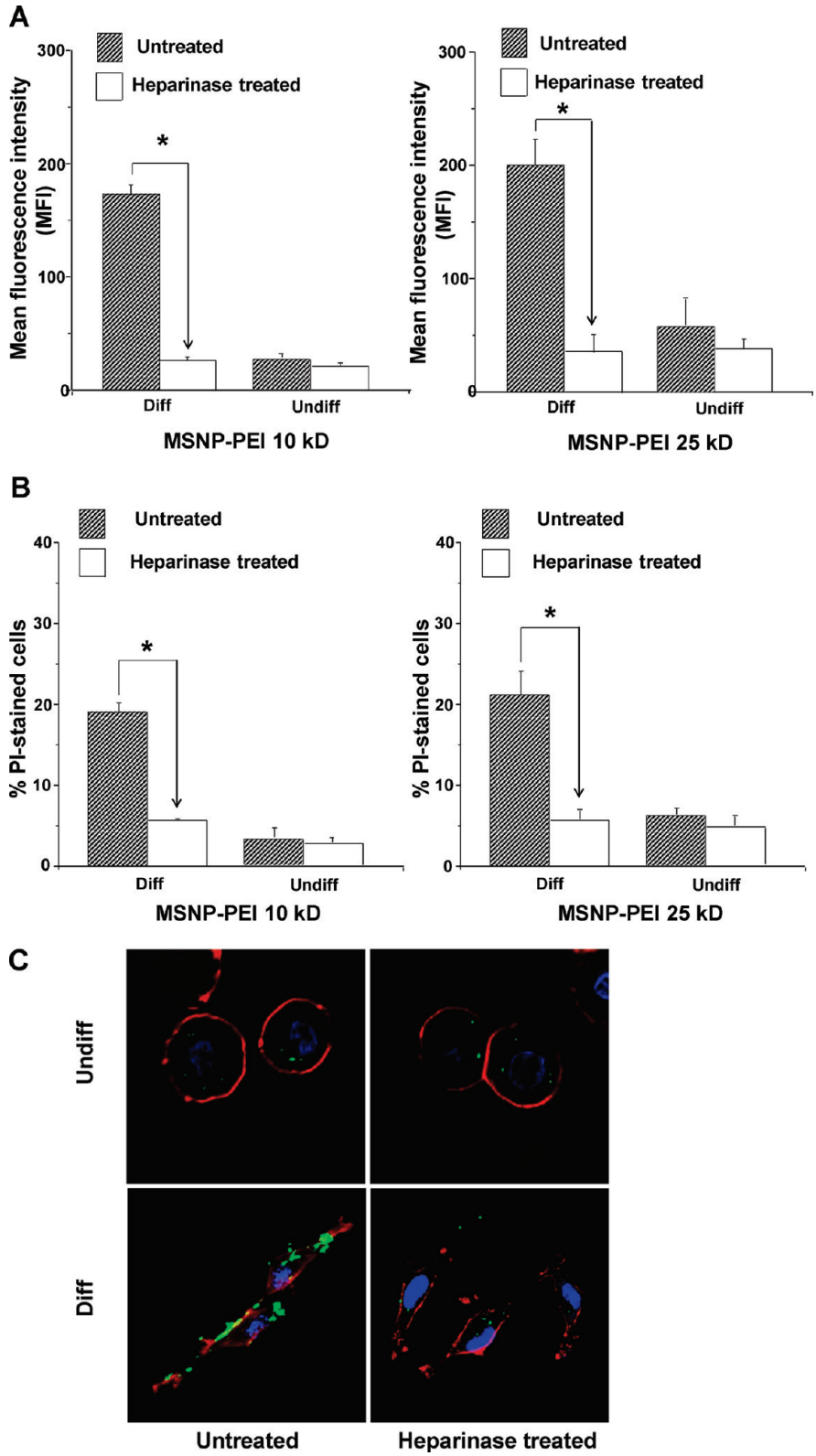

Figure 6. Cellular uptake and cytotoxicity in response to cationic MSNP after heparinase treatment. Undifferentiated and differentiated cells were treated with 5 U of heparinase I/II for 2 h, followed by exposure to FITC-labeled MSNP−PEI 10 kD and 25 kD (25 μg/mL) for 3 h. (A) MFI as determined by flow cytometry shows a 6.4-fold (MSNP−PEI 10 kD) or 6.8-fold (MSNP−PEI 25 kD) decrease in cellular association in heparinase-treated differentiated cells. However, there was no obvious difference in undifferentiated cells. (B) Flow cytometry to assess PI uptake shows a 3.4-fold (MSNP−PEI 10 kD) or 3.7-fold (MSNP−PEI 25 kD) decrease in the % PI stained cells in the differentiated population but no obvious decrease in undifferentiated cells following heparinase treatment. (C) Confocal microscopy showing decreased cell surface binding of FITC-labeled MSNP−PEI 10 kD in differentiated NHBE cells after heparinase treatment. However, there was no obvious difference in undifferentiated NHBE cells. *$p < 0.05$ compared with control.

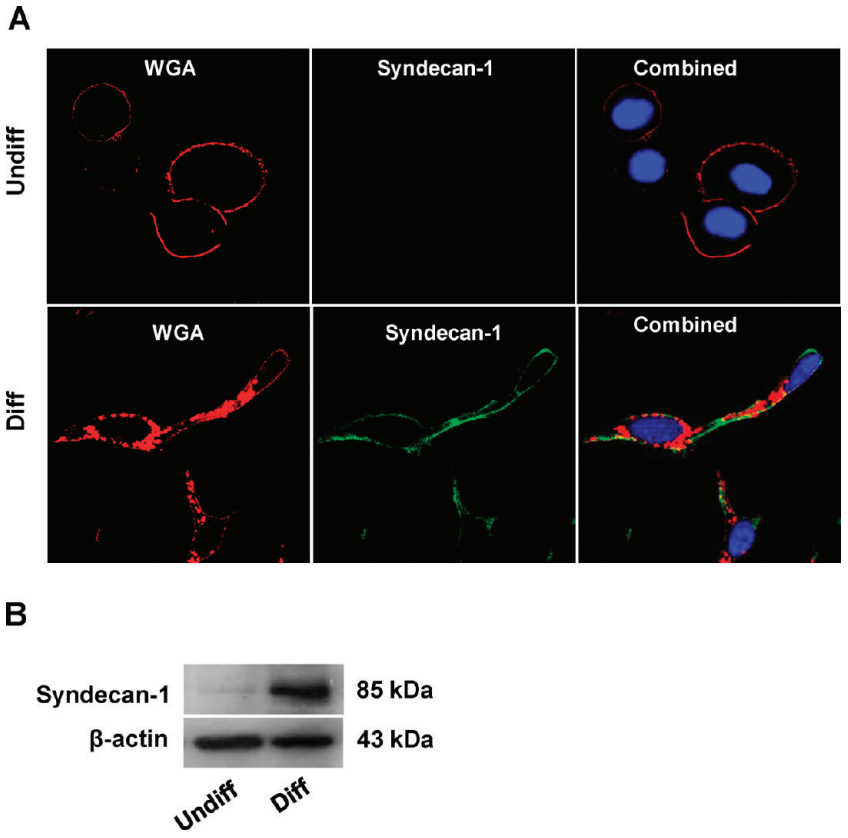

Figure 7. Confocal microscopy and immunoblotting looking at syndecan-1 expression in undifferentiated and differentiated cells. (A) The cell membrane was stained by Alexa Fluor 594-conjugated wheat germ agglutinin, while nuclei were stained with Hoechst 33342. Sydecan-1 was detected by mouse anti-human syndecan-1 monoclonal antibody, which was secondarily detected by a green-fluorescent FITC-labeled goat anti-mouse antiserum. The combined panels on the right-hand side demonstrate that syndecan-1 is abundantly expressed on the surface membrane. (B) Immunoblotting to show the enhanced expression of syndecan-1in differentiated NHBE compared to undifferentiated NHBE cells.

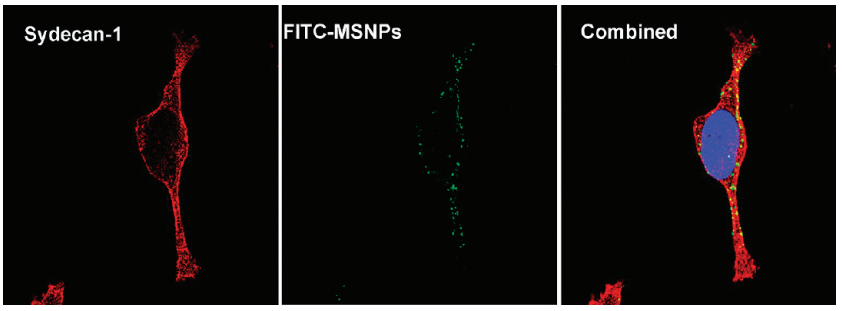

Figure 8. Confocal microscopy to show the co-localization of syndecan-1 with FITC-labeled MSNP−PEI in differentiated cells. Syndecan-1 was detected by an antibody coupled to Alexa Fluor 594 (red fluorescence). FITC-labeled MSNP−PEI 10 kD (25 μg/mL) was added to the cells for 3 h prior to protein and nuclear staining, as in Figure 7A. The combined panel on the right-hand side demonstrates particle co-localizing with syndecan-1. The extent of the co-localization was 64.3% as determined by Image J software.

we show that the state of NHBE cell differentiation determines the cytotoxic effects of cationic MSNP by influencing cellular association, which, in turn, determines perturbation of membrane potential and triggering of injurious intracellular responses. The observation that the differentiation state of a primary cell type can exert an influence on nanoparticle toxicity is an important consideration in choosing primary cells to include in ENM toxicity screening. While the pathophysiological implications of bronchial epithelial cell differentiation in pulmonary toxicity will be discussed below, it is important to consider that the differentiation status of other cell lineages is of importance in evaluating ENM safety. In addition to bronchial epithelial cells, the differentiation status of type I and II alveolar epithelial cells could determine their toxicological response outcomes to environmental insults.[43] Indeed, it has previously been determined that an alveolar type II epithelial

cell line expressing syndecan-1 is capable of binding to a cationic amorphous silica nanoparticle.[32] However, that study did not include a toxicological analysis or a comparison of differentiated to undifferentiated cells. Another cell lineage that needs to be considered in terms of differentiation status in ENM toxicity is myeloid precursors produced in the bone marrow. Monocytes, macrophages, Kuppfer cells, *etc*., are elements of the reticuloendothelial system that could be differentially affected by therapeutic nanoparticles, in which cationic properties lead to *in vivo* toxicity.[27] The same consideration holds for myeloid precursors that populate mucosal surfaces, where macrophages, granulocytes, and dendritic cells may be differentially affected by ENM. In this regard, macrophages have been shown to behave differently from nanoparticles compared to micrometer-sized particles made of the same material.[44] A final example is skin cell differentiation in which better differentiated keratinocytes in the suprabasal layer may differ in their response to ENM from less differentiated cells in the basal layer.[45] In this regard, high-density cationic nanoparticle carriers cause more skin damage than lesser cationic particles during topical noninvasive gene delivery studies.[46]

The pathophysiological significance of cellular differentiation and syndecan-1 expression in the lung lies in the severity and type of pathology that may develop during exposure to cationic nanoparticles. Inhalation of cationic spray paint particles has been shown to induce acute pulmonary edema and bronchiolitis obliterans, which is experimentally reversible by the neutralization of cationic charge.[10] While a variety of intrapulmonary components and physiological conditions can contribute to the development of cationic toxicity, of particular importance is the role of proteoglycans and other membrane components that play a role in surface membrane association of positively charged particles. Physiological and pathophysiological stimuli such as cellular differentiation, oxidative stress, metalloproteinase activity, basic fibroblast growth factor, TGF-β, and pulmonary infections all contribute to syndecan expression.[30,31,47−50] Syndecans are a family of cell surface proteoglycans that play regulatory roles in wound healing, inflammation, and angiogenesis. There are four members of the syndecan family (syndecans-1, -2, -3, and -4), each consisting of an ectodomain carrying heparan sulfate- or chondroitin sulfate-rich glucosaminoglycan chains, a transmembrane domain, and a short cytoplasmic tail.[51] Syndecan-1 is predominantly found on endothelial and epithelial cells, whereas syndecan-4 is ubiquitously expressed.[52] Syndecans are also released as soluble variants that have been found in various body fluids including bronchoalveolar fluid of inflamed lungs.[53−57] Syndecans act as co-receptors that modulate binding and signaling of cytokines, chemokines, and adhesion molecules. Moreover, syndecan-1 cleavage by matrix metalloproteinase 7 helps to establish a gradient for the transepithelial migration of neutrophils into the airway.[58] It has also been established that HSPGs serve as a cellular receptor that binds and promotes the uptake of PEI polymers, TAT protein, and the R_8 peptide.[59] Therefore, it is possible that HSPGs may serve a receptor function for PEI-coated MSNP, leading to particle uptake or retention at the cell surface.

While the specific proportional contribution of syndecan-1 as an anionic surface membrane component to NHBE toxicity is unknown, heparinase treatment virtually eliminated the cytotoxic potential of cationic MSNP (Figure 6). Nonetheless, other HSPGs may also contribute to the exaggerated cationic toxicity in differentiated NHBE cells. Moreover, nonproteinaceous components in the membrane may also contribute to the toxicity, including anionic phospholipid head groups. Membrane fluidity could also play a role as demonstrated by the finding that positively charged polystyrene nanoparticles interact with gellous membrane domains, turning them into a more fluid state, while anionic particles interact with more fluidic membrane domains that develop gelation.[60] Interestingly, the transmembrane and cytoplasmic domains of syndecans play a role in a multistep endocytic pathway that is dependent on detergent-insoluble lipid raft membrane domains.[61]

How does the binding of cationic MSNPs at the surface membrane induce cytotoxicity in NHBE cells, and what is the role of polymer length in these events? In a previous study we have demonstrated that the toxicity of cationic polystyrene nanoparticles (NH_2-PS) in macrophages and bronchial epithelial cells depends on particle endocytosis into the lysosomal compartment, triggering lysosomal injury, mitochondrial perturbation, ROS release, and apoptosis.[13] However, those effects are size dependent and disappeared with particle size > 90 nm. Here we show that larger size cationic MSNPs induce cytotoxicity that manifests as triggering of intracellular calcium flux, mitochondrial membrane depolarization, and ROS production. Moreover, the intracellular response is accompanied by perturbation of surface membrane function and permeability. Whether there is any direct relationship between events at the surface membrane and triggering of intracellular responses is unknown at this stage. While it is possible to link surface membrane perturbation to intracellular responses such as $[Ca^{2+}]_i$ flux and mitochondrial perturbation, this will require further experimentation that falls outside of the scope of the current communication. The syndecans in and of themselves are known to exert effects on cellular signaling, including protein kinase C activation.[62,63]

The observation that high molecular weight PEI polymers are more toxic than particles coated with shorter length polymers is an intriguing finding and of importance in understanding cationic effects at the

nanobio interface. It has been shown previously that the methylene backbone ($-CH_2CH_2N_x-$) as well as the high charge density of high molecular weight PEI polymers play an important role in the toxicity of this material.[64] Moreover, the creation of shorter molecular weight analogues with reduced charge density results in decreased toxicity, to the extent that these analogues can be used for gene delivery.[64] Moreover, we have previously demonstrated that this principle also applies to PEI coating of MSNPs for the purposes of nucleic acid and siRNA delivery to cancer cells.[12] While the complete explanation for the role of polymer length in cellular toxicity still needs further study, it has been shown that differences in the charge density of different molecular weight polymers play a critical role in the ability of PEI to bind and induce flocculation of anionic colloidal silica particles.[28] More specifically, it has been shown that the number of protonated amine groups (cationic charges) in this model is the critical parameter that determines flocculation efficiency, as expressed by a quantitative parameter known as critical flocculation concentration (CFC).[28] The logarithmic derivative of CFC decreases linearly with the increase in polymer molecular weight and also correlates with the distribution of cationic charge on the branched polymer surface. According to this colloidal modeling system, the net cationic charge at contact sites establishes adhesion "patches" that critically define the flocculation behavior.[28] According to this theorem, longer length PEI polymers are capable of increasing the number of adhesion patches with the negatively charged counter surface. We propose that the strength and number of these binding sites also play a role in cell surface events leading to cytotoxicity (Figure S6). Thus, the density distribution rather than the total surface cationic charge would be responsible for the cytotoxic potential (Figure S6). This could explain why, in spite of comparable positive zeta potential (Table 2), MSNPs coated with the longer length PEI polymers are more toxic than the particles coated with shorter length polymers. The situation gets even more interesting when considering the additional formation of a protein corona in a tissue culture medium environment. Surface binding of anionic proteins like BSA could obscure the surface charge during assessment of the electrophoretic mobility of these particles, which assume a negative zeta potential. While the negatively charged corona could exert an important effect on particle behavior in the medium, including determining contact with the cell membrane, these surface interactions could change dynamically once the cellular contact has been established. At this point the protonated amines could compete for binding to negatively charged HSPGs as well as other membrane components. This could lead to a displacement of BSA and a new set of interactions. Whatever the exact explanation is for this complicated interfacial behavior at the nanobio interface, we have demonstrated that stripping of HSPG sulfates with heparinase or neutralizing the number of available amines on the high molecular weight polymers leads to a reduction in cellular association and toxicity. These concepts are of considerable importance to understanding cationic ENM toxicity as well as for the therapeutic use of PEI-coated MSNPs.[12]

Conclusion. The differentiation state of NHBE cells plays a role in shaping the cellular response to cationic mesoporous silica nanoparticles. Differentiated cells capture more of these particles due to high surface expression of a negatively charged HSPG, syndecan-1. This cellular association triggers membrane depolarization and toxicological responses in the cells that could be tracked with our multiparametric screening assay. While it is important to consider the state of cellular differentiation when studying ENM toxicity, it does not mean the results presented here can be generalized to other cell types.

MATERIALS AND METHODS

Chemicals. Tetraethylorthosilicate (TEOS) (98%), cetyltrimethylammonium bromide (CTAB, 95%), 3-(trihydroxysilyl)propyl methylphosphonate (42%), fluorescein isothiocyanate (FITC, 90%), aminopropyltriethoxysilane (APTS, 99%), polyethyleneimine (MW 1.2 and 25 kD), and phthalic anhydride were purchased from Sigma (St. Louis, MO). Polyethyleneimine (MW 0.6, 0.8, 1.8, and 10 kD) were purchased from Alfa Aesar (Ward Hill, MA). All chemicals were reagent grade and used without further purification or modification unless otherwise indicated. Reagent grade water used in all experimental procedures was obtained from a Milli-Q water purification system (Millipore, Bedford, MA).

Synthesis and Attachment of FITC to Mesoporous Silica Nanoparticles. MSNPs were synthesized on the basis of the modified sol–gel process.[12] Typically, 120 mL of cetyltrimethylammonium bromide aqueous solution (5.4 mmol/L) was heated to 80 °C, followed by addition of 875 μL of a NaOH solution (2 mol/L). After stirring for 15 min, 1.25 mL of tetraethylorthosilicate was added dropwise to the CTAB solution. After 15 min stirring, 315 μL of 3-(trihydroxysilyl)propyl methylphosphonate aqueous solution (42% wt) was added to above mixture and stirred for 2 h at 80 °C. The MSNP precipitates were collected by centrifuging at 7800 rpm for 15 min and washed three times with methanol, and the CTAB was extracted by washing in 60 mL of methanol mixed with 2.5 mL of hydrochloric acid (12.1 mol/L). The suspension was refluxed for 12 h, and the MSNPs were collected by centrifuging at 7800 rpm for 15 min, washed three times with methanol, and dispersed in methanol.

Fluorescent-labeled MSNPs were synthesized using the same process except that fluorescein isothiocyanate-TEOS (FITC-TEOS) replaced TEOS. A 1.5 mL amount of FITC dissolved in ethanol (4.0 mmol/L) was mixed with 6 μL of 3-aminopropyltriethoxysilane. The solution was stirred under nitrogen atmosphere for 2 h, followed by addition of 1.25 mL of tetraethylorthosilicate to the mixture.

TABLE 3. Cytotoxicty Markers and Probes Used in the Multiparametric Screening Assay

response marker	fluorescent probe	excitation/emission	response	utility
cell identification/nuclear staining	Hoechst 33342	355/465	nuclear staining	locating and counting cell nuclei
PI uptake	propidium iodide	540/620	increased red fluorescence	compromised cell membrane integrity
intracellular calcium flux	Fluo-4	480/510	increased green fluorescence	increased intracellular calcium level
mitochondrial superoxide	MitoSox Red	510/580	increased red fluorescence	increased superoxide level
hydrogen peroxide	DCF	492/517	increased green fluorescence	increased hydrogen peroxide level
mitochondrial membrane potential	JC-1	480/530	shift of red to green fluorescence	loss of MMP

Polyethyleneimine Coating of MSNPs and Amine Neutralization. Six different PEI polymer sizes (MW 0.6, 0.8, 1.2, 1.8, 10, and 25 kD) were used for MSNP coating. Ten milligrams of particles was dispersed by sonication in 1 mL of ethanol, mixed with 1 mL of PEI (5 mg) in ethanol, and allowed to stir for 30 min. The PEI-coated MSNPs were collected by centrifuging at 15000 rpm for 10 min, then washed with ethanol and phosphate-buffered saline (PBS).

Phthalic anhydride was used to neutralize the PEI amine groups on coated particles. Briefly, 10 mg of PEI-coated MSNP was suspended in 1 mL of anhydrous DMF, followed by the addition of 0.22 mL (for particles coated with 25 kD PEI) or 0.33 mL (for particles coated with 10 kD PEI) of phthalic anhydride solution (10 mg/mL) suspended in anhydrous DMF. The mixture was stirred for 10 h at room temperature, and the neutralized particles were collected by centrifuging at 15 000 rpm for 5 min before washing with DMF, ethanol, and water.

Nanoparticle Dispersion in Cell Culture Media (refs 14 and 16). Nanoparticle stock solutions (5 mg/mL) were prepared by dispersing the dry particles in deionized water through probe sonication (3 W). The stock solution was used to remove 5 μL aliquots, which were mixed with an equal volume of 4% bovine serum albumin (BSA) (Fraction-V, Gemini Bioproducts, USA) and equilibrated for 1 h at room temperature. Cell culture media (1 mL) was added to the BSA-coated nanoparticle suspensions, which were further stabilized by the addition of 2 mg/mL BSA. The nanoparticle suspensions were sonicated (3 W) for 15 s prior to conducting cellular studies.

Physicochemical Characterization. All MSNPs were characterized for size, size distribution, shape, and charge as previously described.[13,14] The shape and structure were characterized using a transmission electron microscope (JEOL JEM 2010, JEOL USA, Inc., Peabody, MA). Microfilms for TEM imaging were made by placing a drop of the respective particle suspension onto a 200-mesh copper TEM grid (Electron Microscopy Sciences, Washington, PA), then drying at room temperature overnight. A minimum of five images were collected to obtain representative views of each particle type. Particle size and zeta potential in solution were measured by using a ZetaSizer Nano (Malvern Instruments Ltd., Worcestershire, UK). Size measurements were performed on dilute particle suspensions in water or complete cell culture media at pH 7.4. The size measurements were made by using dynamic light scattering (DLS) at an angle of 173°. The ZetaSizer Nano was also used to measure the electrophoretic mobility of the MSNPs suspended in solution. Electrophoretic mobility is used as an approximation of particle surface charge and used to calculate zeta potential using the Helmholtz−Smoluchowski equation.

NHBE Culture to Obtain Undifferentiated and Differentiated Cells. Normal human bronchial epithelial cells were purchased from Lonza (Walkersville, MD) and cultured in vented T-75 cm^2 flasks (Corning, Fisher Scientific, Pittsburgh, PA) at 37 °C in a humidified 5% CO_2 atmosphere. The growth medium was bronchial epithelial basal medium (BEBM) (Lonza, Walkersville, MD), supplemented with growth factors from the SingleQuots kit (Lonza, Walkersville, MD) to make BEGM, which contains a retinoic acid (RA) supplement. The culture medium was changed every 48 h until the cells reached 70−80% confluency. Passage 3−5 NHBE cells were used as undifferentiated cells. To obtain differentiated NHBE cells, passage 5 cells were cultured in BEGM free of RA. The medium was changed every 48 h or when the cells reached 70−80% confluency. After 25−30 days in culture, a significant change in cell morphology was observed, namely, a change to spindle shape, which replaced round or elliptic cells. These features were captured by culturing 5×10^4 cells in each well of Lab-Tek 8-well chamber slides (Fisher Scientific, Pittsburgh, PA). Cell nuclei were stained with 5 μg/mL Hoechst 33342, while cell membranes were stained with 5 μg/mL Alexa Fluor 594-conjugated wheat germ agglutinin in PBS for 30 min. Cells were visualized under a 63× objective under a confocal microscope (Leica Confocal 1P/FCS) in the UCLA/CNSI Advanced Light Microscopy/Spectroscopy Shared Facility. Images were processed using Leica Confocal software.

Cell Culture for Transformed Epithelial Cell Lines. Human bronchial epithelial cells, BEAS-2B (ATCC no. CRL-9609), were cultured in BEGM, and rat type I alveolar epithelial cells, R3/1 (a kind gift from Allison Elder from the University of Rochester, and the originator of the R3/1 cells is Roland Koslowski of the Technical University of Dresden, Germany), were cultured in RPMI-1640 supplemented with 10% FBS, 100 U/mL penicillin, 100 μg/mL streptomycin, and 2 mM L-glutamine (complete medium).

Western Blotting Analysis to Confirm the Presence of Epithelial Differentiation Markers (ref 65). Undifferentiated or differentiated cells (2×10^5) were seeded into each well of six-well plates. After overnight growth, cells were washed with PBS and harvested by a scraper blade. The cell pellets were resuspended in cell lysis buffer containing Triton X-100 and protease inhibitors. The lysates were briefly centrifuged and sonicated, and the protein content in the supernatant was measured by the Bradford method. A 50 μg amount of total protein from each sample was electrophoresed by 10% SDS-PAGE and transferred to a PVDF membrane. After blocking, the membranes were incubated with human anti-SPR-2 monoclonal antibody (1:500) (ENZO Life Sciences, Plymouth Meeting, PA) or human anti-β-catenin monoclonal antibody (1:500) (Santa Cruz Biotechnology, Santa Cruz, CA) or human anti-syndecan-1 monoclonal antibody (1:500) (AbD Serotec, Raleigh, NC). The membranes were overlaid with biotinylated secondary antibody (1:1000) before the addition of HRP-conjugated avidin−biotin complex (1:10 000). The proteins were detected using ECL reagent according to the manufacture's instructions.

Use of a Multiparametric Assay to Compare the Cytotoxicity of the Cationic MSNP (ref 16). Five thousand undifferentiated or differentiated NHBE cells or transformed epithelial cells (BEAS-2B or R3/1) in 50 μL of medium were plated into each well of a 384-well plate (Greiner Bio-One, Monroe, NC), followed by overnight growth at 37 °C in a humidified 5% CO_2 incubator. For an outlay of the plate organization, please refer to Figure S7 in the Supporting Information. The medium in each well was aspirated, and 25 μL of noncoated or PEI-coated MSNPs was added into each well. These particles were freshly dispersed in BEGM containing 2 mg/mL BSA plus RA for undifferentiated cells and BEAS-2B or the same medium but without RA for differentiated cells or RPMI-1640 complete medium for R3/1 cells. The plate diagram demonstrates that each nanoparticle was added in quadruplicate at each of the following doses: 0.4, 0.8, 1.6, 3.2, 6.3, 12.5, 25, 100, and 200 μg/mL.

Three cocktails of fluorescent probe mixture were prepared by mixing wavelength-compatible fluorescent probes in BEGM with RA or BEGM without RA.[16] The first cocktail contained Hoechst 33342 (1 μM), Fluo-4 (5 μM), and propidium iodide (5 μM); the second cocktail contained Hoechst 33342 (1 μM), DCF (5 μM), and MitoSox Red (5 μM); and the third cocktail contained Hoechst 33342 (1 μM) and JC-1 (5 μM). The utility of these dyes, their excitation/emission wavelengths, and response profiling are summarized in Table 3. The addition of the cocktails to

individual 384 plates is delineated in Figure S7. Each well received 25 μL of dye mixture for 30 min while being kept under standard cell culture conditions in the dark. Unincorporated dyes were removed by washing, following which tissue culture wells were replenished with BEGM with RA or BEGM without RA (phenol red-free). Epifluorescence readings were obtained hourly for 6 h using an Image-Xpress^{micro} (Molecular Devices, Sunnyvale, CA) equipped with a laser autofocus. DAPI, FITC, and TRITC filter/dichroic combinations were used to image Hoechst 33342 (blue), Fluo-4/DCF/JC-1 (green), and PI/MitoSox Red (red), respectively.[16] Images from the microscope were analyzed using MetaXpress software (Molecular Devices, Sunnyvale, CA) to score % cells positive for each cytotoxicity parameter. Hoechst 33342, which stains all the nuclei, was used to count the total number of cells using the following setting in the blue channel: approximate minimum width was 3 μm (about 3 pixels); the approximate maximum width was 10 μm (about 7 pixels); the threshold intensity above background level was 100 gray levels. In the green (Fluo-4, DCF, and JC-1) and red (PI and MitoSox Red) channels the minimum width was set at 5 μm (about 6 pixels) and the approximate maximum width was 30 μm (about 22 pixels). The threshold intensities above background were set at 250 and 500 gray levels respectively for the green and red channels. The cells regarded as positive were calculated as the % of cells with an above threshold response compared to the total number of Hoechst 33342 positive cells.

The fluorescence data were used for statistical analysis, using a strictly standard mean difference (SSMD) parameter to calculate the difference between test and control samples according to the formula

$$\mathrm{SSMD} = (\mu_{\mathrm{sample}} - \mu_{\mathrm{control}})/\sqrt{{\sigma_{\mathrm{sample}}}^2 + {\sigma_{\mathrm{control}}}^2}$$

where μ_{sample} and μ_{control} are the mean values and σ_{sample} and $\sigma_{\mathrm{control}}$ refer to the standard deviations.[25,26] A heat map was contructed based on the SSMD values, where $|\mathrm{SSMD}| \geq 3$ is equivalent to a probability > 0.99.

Flow Cytometry to Assess the Cellular Association and Cytotoxicity Prior to and after Heparinase Treatment. Cells (5×10^4) in 400 μL of medium were plated in each well of a 48-well plate. After overnight growth at 37 °C in a humidified 5% CO_2 atmosphere, FITC-labeled MSNPs coated with a 10 kD PEI polymer were added for 3 h at a dose of 25 μg/mL. After washing three times in PBS, cells were harvested by trypsinization and analyzed in a LSR flow cytometer using FL-1 and FL-2 to assess FITC and PI fluorescence intensity. PI was incubated with the cells at 5 μg/mL for 30 min. Data were reported as units of mean fluorescence intensity. In order to evaluate the effect of heparinase treatment, differentiated cells were pretreated with 5 U of heparinase I and II (Sigma, St. Louis, MO) for 2 h. After washing in PBS, the cells were treated with the labeled particles.

Confocal Fluorescence Microscopy to Study Cellular Association and Localization of FITC-Labeled and PEI-Coated MSNP with NHBE. The association and cellular distribution of FITC-labeled MSNP−PEI 10 kD with undifferentiated and differentiated cells were assessed by confocal microscopy. Cells (5×10^4) in 400 μL of medium were plated in each well of an 8-well chamber slide. After overnight incubation at 37 °C in a humidified 5% CO_2 atmosphere, the FITC-labeled particles were added at a dose of 25 μg/mL for 3 h. After treatment, cells were washed three times with PBS and fixed in 400 μL of PBS containing 4% paraformaldehyde for 1 h. Cell nuclei were stained with 5 μg/mL Hoechst 33342, while cell membranes were stained with 5 μg/mL Alexa Fluor 594-conjugated wheat germ agglutinin for 30 min. Heparinase-treated cells were also evaluated by the same protocol. Cells were visualized under a confocal microscope (Leica Confocal SP2 1P/FCS) in the UCLA/CNSI Advanced Light Microscopy/Spectroscopy Shared Facility. High-magnification images were obtained with a 63× objective. Optical sections were averaged four times to reduce noise. Images were processed using Leica Confocal software.

Hemolysis Assay (ref 29). Heparinized mouse blood was washed to remove the serum, following which the red blood cells were washed five times with sterile isotonic PBS solution. The RBC were diluted 10× their initial volume in sterile isotonic PBS solution. Then 300 μL of the diluted RBC suspension was mixed with 1200 μL of PBS as a negative control or with 1200 μL of PBS containing 0.025% Triton X-100 as a positive hemolysis control. PEI-coated MSNPs or noncoated particles, suspended in 1200 μL of PBS, were added to the diluted RBC suspension at 25 to 200 μg/mL. The mixtures were vortexed and incubated for 2 h at room temperature. The samples were centrifuged, and the absorbance of the supernatants was measured at 541 nm in a SpectraMax M5 microplate spectrophotometer. The percent hemolysis in each sample was calculated by dividing the difference in absorption between the sample and the negative control by the difference in absorption between the hemolysis positive and negative control, then multiplying this ratio by 100 to obtain % hemolysis.

Assessment of Membrane Potential Using a Fluorescence Method. Membrane potential was assessed using the commercially available FLIPR membrane-potential assay kit from Molecular Devices (Sunnyvale, CA). Briefly, undifferentiated and differentiated cells were seeded into 96-well plates at a density of 5×10^4 cell per well overnight. The adherent cells were washed with PBS and exposed to 100 μL of nanoparticles at concentrations of 6.3, 12.5, 25, 100, and 200 μg/mL for 3 h. Control wells received no particles. Then 100 μL of the assay dye (FMP) was added to each well, followed by 30 min incubation at 37 °C. This dye contains a lipophilic, anionic bis-oxonal component that shows increased cellular fluorescence upon membrane depolarization or fluorescence reduction upon membrane hyperpolarization. Fluorimetric data were collected at room temperature on a SpectraMax M5 microplate spectrophotometer (Molecular Devices, Sunnyvale, CA), with excitation, emission, and cutoff filters set to 530, 565, and 550 nm, respectively. The % change in fluorescence membrane potential was calculated by dividing the difference between the relative fluorescence units (RFU) in nanoparticle-treated cells *vs* control cells by the RFU of the control cells.

Assessment of Syndecan-1 Expression and Co-localization with FITC-Labeled Particles. Syndecan-1 expression was evaluated by confocal microscopy. Cells (5×10^4) in 400 μL of medium were plated in each well of an 8-well chamber slide. After overnight incubation at 37 °C in a humidified 5% CO_2 atmosphere, cells were fixed with 400 μL of PBS containing 4% paraformaldehyde at room temperature for 1 h. After washing and blocking with PBS containing 2% BSA for 1 h, slides were incubated for 30 min with anti-human syndecan-1 monoclonal antibody (AdD Serotec, Raleigh, NC) diluted 1:500 in PBS containing 0.5% BSA. After washing, cells were incubated with 400 μL of FITC-conjugated goat anti-mouse IgG secondary antibody (Santa Cruz Biotechnology, San Cruz, CA) for 30 min. Cell nuclei were stained with 5 μg/mL Hoechst 33342, while cell membranes were stained with 5 μg/mL Alexa Fluor 594-conjugated wheat germ agglutinin for 30 min. Co-localization of syndecan-1 with MSNP−PEI was assessed in the same way except that the cells were incubated with FITC-labeled MSNP−PEI 10 kD for 3 h before fixing, anti-syndecan-1 was added, and then the cells were incubated with the anti-syndecan-1 mAb as above. Cells were washed three times with PBS containing 2% BSA and incubated with 400 μL of Alexa Fluor 594-conjugated goat anti-mouse IgG secondary antibody (Santa Cruz Biotechnology, San Cruz, CA) for 30 min. Cell nuclei were stained with 5 μg/mL Hoechst 33342. Cells were visualized under the confocal microscope as described above.

Statistical Analysis. All data were expressed as mean ± SD. All values were obtained from at least three independent experiments. Statistical significance was evaluated using two-tailed heteroscedastic Student's *t*-tests according to the TTEST function in Microsoft Excel. The difference between groups was considered statistically significant when the *p*-value was less than 0.05.

Acknowledgment. This work is supported by the National Science Foundation and the Environmental Protection Agency under Cooperative Agreement Number DBI-0830117. Any opinions, findings, conclusions, or recommendations expressed herein are those of the author(s) and do not necessarily reflect the views of the National Science Foundation or the

Environmental Protection Agency. This work has not been subjected to an EPA peer and policy review. Key support was provided by the U.S. Public Health Service Grants U19 ES019528 (UCLA Center for Nanobiology and Predictive Toxicology), RO1 CA133697, RO1 ES016746, and RC2 ES018766. Fluorescent microscopy was performed at the CNSI Advanced Light Microscopy/Spectroscopy Shared Facility at UCLA.

Supporting Information Available: PEI content of MSNPs; zeta potentials of neutralized MSNP−PEI; scheme of multiparametric HCS assay; comparison of the PI uptake and MitoSox Red responses in different cells; cell association and cytotoxicity profiling of the different MSNPs; scheme to explain the interaction of PEI polymers on the coated MSNP surface with the cell membrane; layout of the 384-well plates using the fluorescent dye cocktails in the multiparametric HCS assay. This material is available free of charge *via* the Internet at http://pubs.acs.org.

REFERENCES AND NOTES

1. Mastrobattista, E.; van der Aa, M. A.; Hennink, W. E.; Crommelin, D. J. Artificial Viruses: a Nanotechnological Approach to Gene Gelivery. *Nat. Rev. Drug Discovery* **2006,** *5*, 115–121.
2. Allen, T. M.; Cullis, P. R. Drug Delivery Dystems: Entering the Mainstream. *Science* **2004,** *303*, 1818–1822.
3. Nam, J. M.; Thaxton, C. S.; Mirkin, C. A. Nanoparticle-Based Bio-Bar Codes for the Ultrasensitive Detection of Proteins. *Science* **2003,** *301*, 1884–1886.
4. Park, S. J.; Taton, T. A.; Mirkin, C. A. Array-Based Electrical Detection of DNA with Nanoparticle Probes. *Science* **2002,** *295*, 1503–1506.
5. Medintz, I. L.; Uyeda, H. T.; Goldman, E. R.; Mattoussi, H. Quantum Dot Bioconjugates for Imaging, Labelling and Sensing. *Nat. Mater.* **2005,** *4*, 435–446.
6. Lee, D.; Khaja, S.; Velasquez-Castano, J. C.; Dasari, M.; Sun, C.; Petros, J.; Taylor, W. R.; Murthy, N. *In Vivo* Imaging of Hydrogen Peroxide with Chemiluminescent Nanoparticles. *Nat. Mater.* **2007,** *6*, 765–769.
7. Nel, A. E.; Xia, T.; Mädler, L.; Li, N. Toxic Potential of Materials at the Nanolevel. *Science* **2006,** *311*, 622–627.
8. Nel, A. E.; Mädler, L.; Velegol, D.; Xia, T.; Hoek, E. M.; Somasundaran, P.; Klaessig, F.; Castranova, V.; Thompson, M. Understanding Biophysicochemical Interactions at the Nano-Bio Interface. *Nat. Mater.* **2009,** *8*, 543–557.
9. Meng, H.; Xia, T.; George, S.; Nel, A. E. A Predictive Toxicological Paradigm for the Safety Assessment of Nanomaterials. *ACS Nano* **2009,** *3*, 1620–1627.
10. Hoet, P. H.; Gilissen, L.; Nemery, B. Polyanions protect against the *in Vitro* Pulmonary Toxicity of Polycationic Paint Components Associated with the Ardystil Syndrome. *Toxicol. Appl. Pharmacol.* **2001,** *175*, 184–190.
11. Jan, E.; Byrne, S. J.; Cuddihy, M.; Davies, A. M.; Volkov, Y.; Gun'ko, Y. K.; Kotov, N. A. High-Content Screening as a Universal Tool for Fingerprinting of Cytotoxicity of Nanoparticles. *ACS Nano* **2008,** *2*, 928–938.
12. Xia, T.; Kovochich, M.; Liong, M.; Meng, H.; Kabehie, S.; George, S.; Zink, J. I.; Nel, A. E. Polyethyleneimine Coating Enhances the Cellular Uptake of Mesoporous Silica Nanoparticles and Allows Safe Delivery of SiRNA and DNA Constructs. *ACS Nano* **2009,** *3*, 3273–3286.
13. Xia, T.; Kovochich, M.; Liong, M.; Zink, J. I.; Nel, A. E. Cationic Polystyrene Nanosphere Toxicity Depends on Cell-Specific Endocytic and Mitochondrial Injury Pathways. *ACS Nano* **2008,** *2*, 85–96.
14. Xia, T.; Kovochich, M.; Liong, M.; Mädler, L.; Gilbert, B.; Shi, H.; Yeh, J. I.; Zink, J. I.; Nel, A. E. Comparison of the Mechanism of Toxicity of Zinc Oxide and Cerium Oxide Nanoparticles Based on Dissolution and Oxidative Stress Properties. *ACS Nano* **2008,** *2*, 2121–2134.
15. Xia, T.; Kovochich, M.; Brant, J.; Hotze, M.; Sempf, J.; Oberley, T.; Sioutas, C.; Yeh, J. I.; Wiesner, M. R.; Nel, A. E. Comparison of the Abilities of Ambient and Manufactured Nanoparticles to Induce Cellular Toxicity According to an Oxidative Stress Paradigm. *Nano Lett.* **2006,** *6*, 1794–1807.
16. George, S.; Pokhrel, S.; Xia, T.; Gilbert, B.; Ji, Z.; Schowalter, M.; Rosenauer, A.; Damoiseaux, R.; Bradley, K. A.; Mädler, L..;*et al.*Use of a Rapid Cytotoxicity Screening Approach to Engineer a Safer Zinc Oxide Nanoparticle through Iron Doping. *ACS Nano* **2010,** *4*, 15–29.
17. Stern, O. The Theory of the Electrolytic Double-Layer. *Z. Elektrochem. Angew. Phys. Chem.* **1924,** *30*, 508–516.
18. Eisinger, A. L.; Lincoln D. Nadauld, L. D.; Shelton, D. N.; Prescott, S. M.; Diana M. Stafforini, D. M.; Jones, D. A. Retinoic Acid Inhibits β-Catenin through Suppression of Cox-2. *J. Biol. Chem.* **2007,** *282*, 29394–29400.
19. Fujimoto, W.; Marvin, K. W.; George, M. D.; Celli, G.; Darwiche, N.; De Luca, L. M.; Jetten, A. M. Expression of Cornifin in Squamous Differentiating Epithelial Tissues, Including Psoriatic and Retinoic Acid-Treated Skin. *J. Invest. Dermatol.* **1993,** *101*, 268–274.
20. Jetten, A. M.; Bernacki, S. H.; Floyd, E. E.; Saunders, N. A.; Pieniazek, J.; Lotan, R. Expression of a Prepro relaxin-like Gene during Squamous Differentiation of Rabbit Tracheobronchial Epithelial Cells and Its Suppression by Retinoic Acid. *Cell Growth Di*X*er.* **1992,** *3*, 549–556.
21. Lotan, R.; Pieniazek, J.; George, D. D.; Jetten., A. M. Identification of a New Squamous Cell Differentiation Marker and Its Suppression by Retinoids. *J. Cell Physiol.* **1992,** *151*, 94–102.
22. Wilson, V. L.; Harris, C. C. Genomic 5-methyldeoxycytidine Decreases Associated with the Induction of Squamous Differentiation in Cultured Normal Human Bronchial Epithelial Cells. *Carcinogenesis* **1988,** *9*, 2155–2159.
23. Koizumi, H.; Kartasova, T.; Tanaka, H.; Ohkawara, A.; Kuroki, T. Differentiation-Associated Localization of Small Proline-Rich Protein in Normal and Diseased Human Skin. *Br. J. Dermatol.* **1996,** *134*, 686–692.
24. Mucenski, M. L.; Nation, J. M.; Thitoff, A. R.; Besnard, V.; Xu, Y.; Wert, S. E.; Harada, N.; Taketo, M. M.; Stahlman, M. T.; Whitsett, J. A. β-Catenin Regulates Differentiation of Respiratory Epithelial Cells *in Vivo*. *Am. J. Physiol. Lung Cell Mol. Physiol.* **2005,** *289*, L971–L979.
25. Zhang, X. D. A Pair of New Statistical Parameters for Quality Control in RNA Interference High-Throughput Screening Assays. *Genomics* **2007,** *89*, 552–561.
26. Birmingham, A.; Selfors, L. M.; Forster, T.; Wrobel, D.; Kennedy, C. J.; Shanks, E.; Santoyo-Lopez, J.; Dunican, D. J.; Long, A.; Kelleher, D..;*et al.*Statistical Methods for Analysis of High-Throughput RNA Interference Screens. *Nat. Methods* **2009,** *6*, 569–575.
27. McNeil, S. E. Nanoparticle Therapeutics: a Personal Perspective. *Wiley Interdiscip. Rev. Nanomed. Nanobiotechnol.* **2009,** *1*, 264–271.
28. Lindquist, G. M.; Stratton, R. A. The Role of Polyelectrolyte Charge Density and Molecular Weight on the Absorption and Flocculation of Colloidal Silica with Polyethylenimine. *J. Colloid Interface Sci.* **1976,** *55*, 45–59.
29. Slowing, I. I.; Wu, C. W.; Vivero-Escoto, J. L.; Lin, V. S. Mesoporous Silica Nanoparticles for Reducing Hemolytic Activity Towards Mammalian Red Blood Cells. *Small* **2009,** *5*, 57–62.
30. Bishop, J. R.; Schuksz, M.; Esko, J. D. Heparan Sulphate Proteoglycans Fine-Tune Mammalian Physiology. *Nature* **2007,** *446*, 1030–1037.
31. Cool, S. M.; Nurcombe, V. Heparan Sulfate Regulation of Progenitor Cell Fate. *J. Cell Biochem.* **2006,** *99*, 1040–1051.
32. Orr, G.; Panther, D. J.; Cassens, K. J.; Phillips, J. L.; Tarasevich, B. J.; Pounds, J. G. Syndecan-1 Mediates the Coupling of Positively Charged Submicrometer Amorphous Silica Particles with Actin Filaments across the Alveolar Epithelial Cell Membrane. *Toxicol. Appl. Pharmacol.* **2009,** *236*, 210–220.
33. Mislick, K. A.; Baldeschwieler, J. D. Evidence for the Role of Proteoglycans in Cation-Mediated Gene Transfer. *Proc. Natl. Acad. Sci. U. S. A.* **1996,** *93*, 12349–12354.
34. Kopatz, I.; Remy, J. S.; Behr, J. P. A Model for Non-Viral Gene Delivery: Through Syndecan Adhesion Molecules and Powered by Actin. *J. Gene Med.* **2004,** *6*, 769–776.

35. Bausinger, R.; Gersdorff, K.; Braeckmans, K.; Ogris, M.; Wagner, E.; Bräuchle, C.; Zumbusch, A. The Transport of Nanosized Gene Carriers Unraveled by Live-Cell Imaging. *Angrew. Chem., Int. Ed.* **2006,** *45*, 1568–1572.
36. Couchman, J. R. Syndecans: Proteoglycan Regulators of Cell-Surface Microdomains?. *Nat. Rev. Mol. Cell Biol.* **2003,** *4*, 926–937.
37. Zhang, L.; Esko, J. D. Amino Acid Determinants that Drive Heparan Sulfate Assembly in a Proteoglycan. *J. Biol. Chem.* **1994,** *269*, 19295–19299.
38. Brown, T. A.; Bouchard, T.; John, T., St.; Wayner, E.; Carter, W. G. Human Keratinocytes Express a New CD44 Core Protein (CD44E) as a Heparan-Sulfate Intrinsic Membrane Proteoglycan with Additional Exons. *J. Cell Biol.* **1991,** *113*, 207–221.
39. Perrimon, N.; Bernfield, M. Specificities of Heparan Sulphate Proteoglycans in Developmental Processes. *Nature* **2000,** *404*, 725–728.
40. Paris, S.; Burlacu, A.; Durocher, Y. Opposing Roles of Syndecan-1 and Syndecan-2 in Polyethyleneimine-Mediated Gene Delivery. *J. Biol. Chem.* **2008,** *283*, 7697–7704.
41. Oberdörster, G.; Maynard, A.; Donaldson, K.; Castranova, V.; Fitzpatrick, J.; Ausman, K.; Carter, J.; Karn, B.; Kreyling, W.; Lai, D.; *et al.* Principles for Characterizing the Potential Human Health Effects from Exposure to Nanomaterials: Elements of a Screening Strategy. *Part. Fibre Toxicol.* **2005,** *2*, 8.
42. Eglen, R. M.; Gilchrist, A.; Reisine, T. An Overview of Drug Screening Using Primary and Embryonic Stem Cells. *Comb. Chem. High Throughput Screen.* **2008,** *11*, 566–572.
43. Narasaraju, T. A.; Chen, H.; Weng, T.; Bhaskaran, M.; Jin, N.; Chen, J.; Chen, Z.; Chinoy, M. R.; Liu, L. Expression Profile of IGF System During Lung Injury and Recovery in Rats Exposed to Hyperoxia: a Possible Role of IGF-1 in Alveolar Epithelial Cell Proliferation and Differentiation. *J. Cell Biochem.* **2006,** *97*, 984–998.
44. Donaldson, K.; Brown, D.; Clouter, A.; Duffin, R.; MacNee, W.; Renwick, L.; Tran, L.; Stone, V. The Pulmonary Toxicology of Ultrafine Particles. *J. Aerosol. Med.* **2002,** *15*, 213–220.
45. Sanderson, R. D.; Hinkes, M. T.; Bernfield, M. Syndecan-1, a Cell-Surface Proteoglycan, Changes in Size and Abundance when Keratinocytes Stratify. *J. Invest. Dermatol.* **1992,** *99*, 390–396.
46. Badea, I.; Wettig, S.; Verrall, R.; Foldvari, M. Topical Non-Invasive Gene Delivery Using Gemini Nanoparticles in Interferon-Gamma-Deficient Mice. *Eur. J. Pharm. Biopharm.* **2007,** *65*, 414–422.
47. Kliment, C. R.; Englert, J. M.; Gochuico, B. R.; Yu, G; Kaminski, N.; Rosas, I; Oury, T. D. Oxidative Stress Alters Syndecan-1 Distribution in Lungs with Pulmonary Fibrosis. *J. Biol. Chem.* **2009,** *284*, 3537–3545.
48. Chen, P.; Abacherli, L. E; Nadler, S. T.; Wang, Y.; Li, Q.; Parks, W. C. MMP7 Shedding of Syndecan-1 Facilitates Re-epithelialization by Affecting alpha(2)beta(1) Integrin Activation. *PLoS One* **2009,** *4*, e6565.
49. Romarís, M.; Bassols, A.; David, G. Effect of Transforming Growth Factor-beta 1 and Basic Fibroblast Growth Factor on the Expression of Cell Surface Proteoglycans in Human Lung Fibroblasts. Enhanced Glycanation and Fibronectin-binding of CD44 Proteoglycan, and Down-regulation of Glypican. *Biochem. J.* **1995,** *310*, 73–81.
50. Wang, S. H.; Zhang, C.; Liao, C. P.; Lasbury, M. E.; Durant, P. J.; Tschang, D.; Lee, C. H. Syndecan-1 Expression in the Lung during Pneumocystis Infection. *J. Eukaryot. Microbiol.* **2006,** *53*, S122–123.
51. Bartlett, A. H.; Hayashida, K.; Park, P. W. Molecular and Cellular Mechanisms of Syndecans in Tissue Injury and Inflammation. *Mol. Cells* **2007,** *24*, 153–166.
52. Kim, C. W.; Goldberger, O. A.; Gallo, R. L.; Bernfield, M. Members of the Syndecan Family of Heparan Sulfate Proteoglycans are Expressed in Distinct Cell-, Tissue-, and Development-specific Patterns. *Mol. Biol. Cell* **1994,** *5*, 797–805.
53. Seidel, C.; Sundan, A.; Hjorth, M.; Turesson, I.; Dahl, I. M.; Abildgaard, N.; Waage, A.; Borset, M. Serum Syndecan-1: a New Independent Prognostic Marker in Multiple Myeloma. *Blood* **2000,** *95*, 388–392.
54. Subramanian, S. V.; Fitzgerald, M. L.; Bernfield, M. Regulated Shedding of Syndecan-1 and -4 Ectodomains by Thrombin and Growth Factor Receptor Activation. *J. Biol. Chem.* **1997,** *272*, 14713–14720.
55. Joensuu, H.; Anttonen, A.; Eriksson, M.; Mäkitaro, R.; Alfthan, H.; Kinnula, V.; Leppä, S. Soluble Syndecan-1 and Serum Basic Fibroblast Growth Factor Are New Prognostic Factors in Lung Cancer. *Cancer Res.* **2002,** *62*, 5210–5217.
56. Hasegawa, M.; Betsuyaku, T.; Yoshida, N.; Nasuhara, Y.; Kinoshita, I.; Ohta, S.; Itoh, T.; Park, P. W.; Nishimura, M. Increase in Soluble CD138 in Bronchoalveolar Lavage Fluid of Multicentric Castleman's Disease. *Respirology* **2007,** *12*, 140–143.
57. Penc, S. F.; Pomahac, B.; Winkler, T.; Dorschner, R. A.; Eriksson, E.; Herndon, M.; Gallo, R. L. Dermatan Sulfate Released after Injury Is a Potent Promoter of Fibroblast Growth Factor-2 Function. *J. Biol. Chem.* **1998,** *273*, 28116–28121.
58. Li, Q.; Park, P. W.; Wilson, C. L.; Parks, W. C. Matrilysin Shedding of Syndecan-1 Regulates Chemokine Mobilization and Transepithelial Efflux of Neutrophils in Acute Lung Injury. *Cell* **2002,** *111*, 635–646.
59. Poon, G. M.; Gariépy, J. Cell-Surface Proteoglycans as Molecular Portals for Cationic Peptide and Polymer Entry into Cells. *Biochem. Soc. Trans.* **2007,** *35*, 788–793.
60. Wang, B.; Zhang, L.; Bae, S. C.; Granick, S. Nanoparticle-Induced Surface Reconstruction of Phospholipid Membranes. *Proc. Natl. Acad. Sci. U. S. A.* **2008,** *105*, 18171–18175.
61. Fuki, I. V.; Meyer, M. E.; Williams, K. J. Transmembrane and Cytoplasmic Domains of Syndecan Mediate a Multi-step Endocytic Pathway Involving Detergent-Insoluble Membrane Rafts. *Biochem. J.* **2000,** *351*, 607–612.
62. Beauvais, D. M.; Rapraeger, A. C. Syndecan-1-Mediated Cell Spreading Requires Signaling by $\alpha_v\beta_3$ Integrins in Human Breast Carcinoma cells. *Exp. Cell Res.* **2003,** *286*, 219–232.
63. Oh, E. S.; Woods, A.; Couchman, J. R. Syndecan-4 Proteoglycan Regulates the Distribution and Activity of Protein Kinase C. *J. Biol. Chem.* **1997,** *272*, 8133–8136.
64. Xiong, M. P.; Forrest, M. L.; Ton, G.; Zhao, A.; Davies, N. M.; Kwon, G. S. Poly(aspartate-g-PEI800), a Polyethylenimine Analogue of Low Toxicity and High Transfection Efficiency for Gene Delivery. *Biomaterials* **2007,** *28*, 4889–4900.
65. Li, N.; Alam, J.; Venkatesan, M. I.; Eiguren-Fernandez, A.; Schmitz, D.; Di Stefano, E.; Slaughter, N.; Killeen, E.; Wang, X.; Huang, A.; *et al.* Nrf2 is a Key Transcription Factor that Regulates Antioxidant Defense in Macrophages and Epithelial Cells: Protecting against the Proinflammatory and Oxidizing Effects of Diesel Exhaust Chemicals. *J. Immunol.* **2004,** *173*, 3467–3481.